Comparative Analysis of Linear vs. Nonlinear Multi-Period OPF Models for Active Distribution Systems

Aryan Ritwajeet Jha∗, *SIEEE*, Subho Paul†, *MIEEE*, and Anamika Dubey∗, *SMIEEE*
∗*School of Electrical Engineering & Computer Science*, *Washington State University*, Pullman, WA, USA
†*Department of Electrical Engineering*, *Indian Institute of Technology (BHU) Varanasi*, Varanasi, UP, India
∗{aryan.jha, anamika.dubey}@wsu.edu, †{subho.eee}@itbhu.ac.in

***Abstract*—**

***Index Terms*—Battery energy storage systems, distribution system, optimal power flow, distributed energy resources.**

I. Introduction

II. Problem Formulation

A. Notations

In this study, the distribution system is modeled as a tree (connected graph) with N number of buses (indexed with i, j, and k); the study is conducted for T time steps (indexed by t), each of interval length Δt. The sets of buses with DERs and batteries are D and B respectively, such that $D, B \subseteq N$. A directed edge from bus i to j in the tree is represented by ij and the set for edges is given by $\mathcal{L}$. Line resistance and reactance are r_{ij} and x_{ij}, respectively. Magnitude of the current flowing through the line at time t is denoted by I_{ij}^t and $l_{ij}^t = \left(I_{ij}^t\right)^2$. The voltage magnitude of bus j at time t is given by V_j^t and $v_j^t = \left(V_j^t\right)^2$. Apparent power demand at a node j at time t is $s_{L_j}^t$ $(= p_{L_j}^t + jq_{L_j}^t)$. The active power generation from the DER present at bus j at time t is denoted by $p_{D_j}^t$ and controlled reactive power dispatch from the DER inverter is $q_{D_j}^t$. DER inverter capacity is $S_{D_{R_j}}$. The apparent power flow through line ij at time t is S_{ij}^t $(= P_{ij}^t + jQ_{ij}^t)$. The real power flowing from the substation into the network is denoted by P_{Subs}^t and the associated cost involved per kWh is C^t. The battery energy level is B_j^t. Charging and discharging active power from battery inverter (of apparent power capacity $S_{B_{R_j}}$) are denoted by $P_{c_j}^t$ and $P_{d_j}^t$, respectively and their associated efficiencies are η_c and η_d, respectively. The energy capacity of the batteries is denoted by B_{R_j}, and the rated battery power is $P_{B_{R_j}}$. soc_{min} and soc_{max} are fractional values for denoting safe soc limits of a battery about its rated state-of-charge (soc) capacity. The reactive power support of the battery inverter is indicated by $q_{B_j}^t$.

B. MPCOPF with Batteries

The OPF problem aims to minimize two objectives as shown in (1). The first term in (1) aims to minimize the total energy cost for the entire horizon. Including the 'Battery Loss' cost as the second term ($\alpha > 0$) helps eliminate the need for binary (integer) variables typically used to prevent simultaneous charging and discharging. The resulting OPF problem is a non-convex optimization problem [1].

$$\min \sum_{t=1}^{T} \Bigg[C^t P_{Subs}^t \Delta t + \alpha \sum_{j \in \mathcal{B}} \Big\{ (1-\eta_C) P_{C_j}^t + \left(\frac{1}{\eta_D} - 1 \right) P_{D_j}^t \Big\} \Bigg] \tag{1}$$

Subject to the constraints (2) to (12) as given below:

$$\sum_{(j,k)\in\mathcal{L}} \left\{P_{jk}^t\right\} - \left(P_{ij}^t - r_{ij} l_{ij}^t\right) = \left(P_{d_j}^t - P_{c_j}^t\right) + p_{D_j}^t - p_{L_j}^t \tag{2}$$

$$\sum_{(j,k)\in\mathcal{L}} \left\{Q_{jk}^t\right\} - \left(Q_{ij}^t - x_{ij} l_{ij}^t\right) = q_{D_j}^t + q_{B_j}^t - q_{L_j}^t \tag{3}$$

$$v_j^t = v_i^t - 2(r_{ij} P_{ij}^t + x_{ij} Q_{ij}^t) + \left\{r_{ij}^2 + x_{ij}^2\right\} l_{ij}^t \tag{4}$$

$$(P_{ij}^t)^2 + (Q_{ij}^t)^2 = l_{ij}^t v_i^t \tag{5}$$

$$P_{Subs}^t \geq 0 \tag{6}$$

$$v_j^t \in \left[V_{min}^2, V_{max}^2\right] \tag{7}$$

$$q_{D_j}^t \in \left[-\sqrt{{S_{D_{R,j}}}^2 - {p_{D_j}^t}^2}, \sqrt{{S_{D_{R,j}}}^2 - {p_{D_j}^t}^2} \right] \tag{8}$$

$$B_j^t = B_j^{t-1} + \Delta t \eta_c P_{c_j}^t - \Delta t \frac{1}{\eta_d} P_{d_j}^t \tag{9}$$

$$P_{c_j}^t, P_{d_j}^t \in \left[0, P_{B_{R_j}}\right], \quad B_j^0 = B_j^T \tag{10}$$

$$q_{B_j}^t \in \left[-\sqrt{0.44} P_{B_{R,j}}, \sqrt{0.44} P_{B_{R,j}} \right] \tag{11}$$

$$B_j^t \in \left[soc_{min} B_{R,j}, soc_{max} B_{R,j} \right] \tag{12}$$

A branch power flow model, given by (2) to (5), is used to represent power flow in distribution system. Constraints (2) and (3) model the active and reactive power balance at node j, respectively. The KVL equation for branch (ij) is represented by (4), while the equation describing the relationship between current magnitude, voltage magnitude and apparent power magnitude for branch (ij) is given by (5). Backflow of real power into the substation from the distribution system is avoided using the constraint (6). The allowable limits for bus voltages are modeled via (7). (8) describes the reactive power

TABLE I: Parameter values

Parameter	Value
V_{min}, V_{max}	0.95 pu, 1.05 pu
$p_{D_{R_j}}$	$0.33p_{L_{R_j}}$
$S_{D_{R_j}}$	$1.2p_{D_{R_j}}$
$P_{B_{R_j}}$	$0.33p_{L_{R_j}}$
$S_{B_{R_j}}$	$1.2P_{B_{R_j}}$
B_{R_j}	$T_{fullCharge} \times P_{B_{R_j}}$
$T_{fullCharge}$	4 h
Δt	1 h
η_c, η_d	0.95, 0.95
soc_{min}, soc_{max}	0.30, 0.95
α	0.001

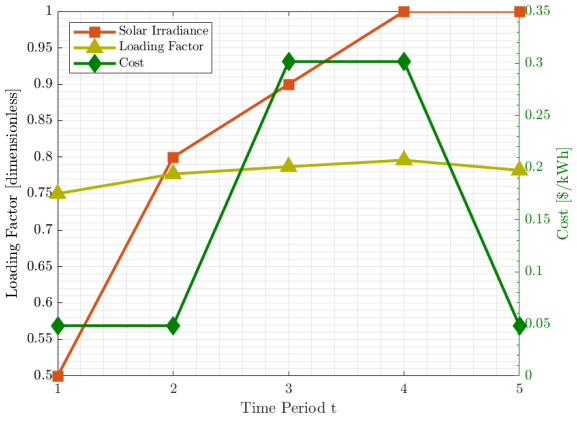

Fig. 1: Forecasts for demand power, irradiance and cost of substation power over a 5 hour horizon

limits of DER inverters. The trajectory of the battery energy versus time is given by (9) (this is a time-coupled constraint). Battery charging and discharging powers are limited by the battery's rated power capacity, as given by (10). (10) also says that the initial and final energy levels for battery must be the same at the end of the optimization time horizon. Every battery's reactive power is also constrained by the corresponding inverter's rated capacity, modeled in (11). For the safe and sustainable operation of the batteries, the energy B_j^t is constrained to be within some percentage limits of the rated battery SOC capacity, modeled using (12)

III. Case Study Demonstration

In the following subsections, the proposed MPDOPF algorithm is compared against the MPCOPF algorithm in terms of resultant optimal control variables, optimality gap in the objective function, and computational performance. Secondly, the resultant control variables are tested for ACOPF feasibility against OpenDSS. Section III-A describes the comparison over a 5 hour horizon with an additional focus on describing the workflow of the MPDOPF algorithm. Section III-B describes the comparison over a 10 hour horizon to test for the scalability of the MPDOPF algorithm.

TABLE II: Comparative analyses between MPCOPF and MPDOPF - 5 time-period horizon

Metric	MPCOPF	MPDOPF
Largest subproblem		
Decision variables	3150	1320
Linear constraints	5831	2451
Nonlinear constraints	635	265
Simulation results		
Substation power cost ($)	576.31	576.30
Substation real power (kW)	4308.28	4308.14
Line loss (kW)	75.99	76.12
Substation reactive power (kVAR)	574.18	656.24
PV reactive power (kVAR)	116.92	160.64
Battery reactive power (kVAR)	202.73	76.01
Computation		
Number of Iterations	-	5
Total Simulation Time (s)	521.25	49.87

A. Simulation Results

Table II depicts a comparison between MPCOPF and MPDOPF in their problem scope, results and computational performance.

1) Largest Subproblem vs. Computational Performance: This first section of the Table II, 'largest subproblem' provides specifics of the 'computational bottleneck' encountered by either algorithm during its course. As described in **??**, the bottleneck represents the OPF subproblem which is computationally the most intensive and thus is a key indicator of the expected time the algorithm will take to complete. As can be seen in the third section 'Computation', there is more than a 10x speedup in computation time with MPDOPF, even though 5 such iterations were performed, totalling to 20 OPF calls over the 4 areas of the test system.

2) Optimality of Objective Function and Control Variables: The second section of the Table II i.e. 'Simulation results' showcases that MPDOPF provides almost zero optimality gap (same values for Substation Power Cost, the objective function). Interestingly, there is a significant difference in the suggested optimal reactive power control values for inverters associated with DERs and batteries (results aggregated over all components over the horizon for conciseness). This highlights the fact that a nonconvex nonlinear optimization problem may not necessarily have a unique global optimal point. There is a possibility of having multiple feasible solutions with the same objective function value.

3) ACOPF Feasibility Analysis: Table III showcases the ACOPF feasibility of the control values suggested by the MPDOPF algorithm. The first section 'Full horizon' describes the respective output variables for the entire horizon from MPDOPF and OpenDSS. The second section 'Max. all-time discrepancy' stores the highest discrepancy between key state/output variables for all components across any time between MPDOPF and OpenDSS. In both sections, the discrepancies are small enough to warrant the feasibility of the obtained solution.

TABLE III: ACOPF feasibility analyses - 5 hour

Metric	MPDOPF	OpenDSS
Full horizon		
Substation real power (kW)	4308.14	4308.35
Line loss (kW)	76.12	76.09
Substation reactive power (kVAR)	656.24	652.49
Max. all-time discrepancy		
Voltage (pu)	0.0002	
Line loss (kW)	0.0139	
Substation power (kW)	0.3431	

To ensure that battery charging and discharging complementarity is respected without relying on integer constraints, the battery charging and discharging profiles were carefully examined. The results confirm this complementarity, as illustrated in **??** as one such example.

4) Workflow Analysis: The workflow of the MPDOPF algorithm, which involves the exchange of boundary variables between parent-child area pairs, is illustrated in the convergence plots in **????**. Each line graph represents a specific time period for both plots. Similarly, **??** shows the convergence of the objective function towards its optimal value over successive iterations. From these plots, we observe that although the decision variables may initially deviate from their optimal values, they gradually approach optimality with each rolling iteration, converging after 5 macro iterations in this instance.

B. Scalability Analysis

To demonstrate the scalability of the proposed algorithm, additional simulations were conducted over a 10-hour time horizon. **??** shows the forecasted profiles for load, solar irradiance and cost of substation power over the 10-hour horizon. The simulation results are summarized in Table IV and Table V.

From the comparison against MPCOPF in Table IV, it can again be seen that MPDOPF is able to converge to the same optimal solution as MPCOPF. The computational speed up is even more pronounced than for the 5 time-period simulation. It was observed that the solution time for MPCOPF increased significantly with the length of the study horizon, whereas the increase in solution time for MPDOPF was comparatively smaller. This indicates that the proposed spatially distributed MPOPF framework is scalable to a certain extent.

TABLE IV: Comparison between MPCOPF and MPDOPF - 10 hour

Metric	MPCOPF	MPDOPF
Largest subproblem		
Decision variables	6300	2640
Linear constraints	11636	4891
Nonlinear constraints	1270	530
Simulation results		
Substation power cost ($)	1197.87	1197.87
Substation real power (kW)	8544.28	8544.04
Line loss (kW)	148.67	148.94
Substation reactive power (kVAR)	1092.39	1252.03
PV reactive power (kVAR)	222.59	139.81
Battery reactive power (kVAR)	388.52	310.94
Computation		
Number of Iterations	-	5
Total Simulation Time (s)	4620.73	358.69

TABLE V: ACOPF feasibility analyses - 10 hour

Metric	MPDOPF	OpenDSS
Full horizon		
Substation real power (kW)	8544.04	8544.40
Line loss (kW)	148.94	148.87
Substation reactive power (kVAR)	1252.03	1243.36
Max. all-time discrepancy		
Voltage (pu)	0.0002	
Line loss (kW)	0.0132	
Substation power (kW)	0.4002	

Again, as can be seen in Table V comparison against OpenDSS has yielded small discrepancies, attesting to the feasibility of the solution.

IV. Conclusions

This study aims to develop a computationally-efficient approach to solve multi-period optimal power flow problems (MPOPF) in distribution systems to coordinate DERs and BESS. Specifically, the authors propose a spatially distributed approach utilizing the ENApp algorithm to solve the MPOPF problem. The effectiveness of the proposed distributed algorithm is validated via simulations on the IEEE 123 bus test system. Simulation results demonstrate that the proposed distributed approach achieves solutions that are AC-feasible and nearly optimal (approaching the solutions obtained from equivalent centralized formulations), while significantly reducing computational costs. This highlights the efficacy of spatial decomposition in reducing solution times for MPOPF problems. However, it is important to note that even the proposed spatially distributed MPOPF algorithm encounters computational complexities when optimizing over longer time horizons. In the future, the authors plan to investigate integrating spatial and temporal decomposition techniques to address scalability issues in time-coupled multi-period OPF problems.

V. Acknowledgement

The authors acknowledge the financial support provided by the Department of Energy (DOE) for the project named 'Spokane Connected Communities' under contract number DE-EE0009775.

References

[1] N. Nazir and M. Almassalkhi, "Guaranteeing a Physically Realizable Battery Dispatch Without Charge-Discharge Complementarity Constraints," IEEE Trans. Smart Grid, vol. 14, no. 3, pp. 2473–2476, Sep. 2021.